Electronic Supplementary Material (ESI) for RSC Advances.

Supporting Information

for

Fabrication, Gradient Extraction and Surface Polarity-Dependent Photoluminescence of Cow Milk-Derived Carbon Dots

*Shuai Han, He Zhang, Jian Zhang, Yujie Xie, Liangliang Liu, Hangxing Wang, Xiangkai Li, Weisheng Liu, Yu Tang**

Table of contents in Supporting Information:

15. Figure S13. The possible mechanism of separating CMCD using "gradient extraction" process.

16. Figure S14. The UV/Vis spectra of the four E-CMCD fractions in aqueous solution.

17. Table S2 Summary of luminescence properties of the four E-CMCD fractions in aqueous solution.

18. Figure S15. The cyclic voltammogram of the E-CMCD and 0.1 mol/L KCl aqueous solution.

19. Figure S16. Excitation-dependent PL intensities of the four E-CMCD fractions.

20. Figure S17. Fluorescence decay curve of the four E-CMCD fractions recorded at room temperature in aqueous solution. **Note:** The emission decay curve was monitored under the excitation wavelength at 360 nm, and the curves all can be fitted by triexponential functions.

21. Figure S18. The PL behavior of the four CMCD fractions in different pH conditions.

1. Experimental section.

Preparation of cow milk-derived carbon dots (CMCD). CMCD were prepared by hydrothermal treatment of diluted cow milk. In a typical synthesis, cow milk (5 mL) was diluted by adding DI-water (25 mL), and the mixture was transferred to a 50 mL Teflon-lined stainless steel autoclave for hydrothermal treatment at 180°C for a period of 12 h. The CMCD were collected by removing the large dots though centrifugation at 11000 rpm for 5 min, and then the suspension was filtered through a 0.22 μm microporous membrane, yielding a yellow solution. The CMCD solution thus obtained was diluted to 50 mL with DI-water for further separation.

The "gradient extraction" process. The CMCD obtained were separated by gradient extraction with organic solvents in gradation of increasing polarity. Typically, About 25mL organic solvent of hexane (polarity: 0.06); carbon tetrachloride (polarity: 1.6); mixture of carbon tetrachloride and dichloromethane (v:v = 3:2); dichloromethane (polarity: 3.4) were used to extract the corresponding surface-polarity CMCD in turn *(yield: 0.4%, 1.1%, 2.4%, 5%; the yields of CMCD with different surface characteristics might be influenced by the reaction conditions and the chemical composition of the carbon source*[S1]). The organic solvent was removed by rotary evaporation, and the residues were dried in vacuum at 35 centigrade for 24 h. At last, the dry CMCD fractions were redispersed in DI-water for optical properties.

Notes: It is worth to mention that it is very important to select appropriate solvent system in the gradient extraction. In the experiment design, the effects of some factors were considered as follows: Firstly, it is needed to be no aromatic structures in the organic solvent molecules, which might cause aromatic ring stacking interactions with CMCD surfaces. Secondly, it is needed to be no heteroatoms (such as "O", "N") in the organic solvent molecules, which might cause hydrogen bonding with the CMCD surfaces and affect the precision of XPS results. Thirdly, chloroform is more toxic than dichloromethane, so dichloromethane is chosen to be the strong polar solvent in the gradient extraction process. Fourthly, the blending ratio of the mixed *solvent was considered to be "3:2" as the optimum conditions by a series of contrast experiments. Fifthly, after the gradient extraction, there were still much CMCD remained in the aqueous solution, and we assumed that the residual CMCD were too hydrophilic to be extracted by the organic solvents. Because the residual CMCD held a large percent of the raw CMCD (91 %), so the surface characteristics of these CMCD were similar with the raw CMCD.*

2.

Table S1 The nutritional content of the cow milk

	Energy	Protein	Fat	Carbohydrate	Sodium
Content	3%	5%	6%	2%	3%

Data notes:

The element analysis result of the dry milk: C, 4.09 %; N, 52.01%; H, 7.50%.

3.

Figure S1. The FTIR contrastive analysis of the obtained cow milk-derived carbon dots (CMCD) at different reaction times.

4.

Figure S2. The photoluminescence intensities contrastive analysis of the obtained CMCD at different reaction times.

Data notes:

In fact, the formation process of carbon dots (CD) from bioresources is complicated and a clear scheme has not yet been reported. It could be seen that cow milk is nutrient-rich carbon source from Table S1, and the mechanism for synthesis of CMCD may involve denaturing, breakage, and carbonization of its constituents.[S2] It is worth noting that the intensity of the peaks associated with N-H, O-H, and C=O groups gradually increased with increasing reaction time from the FTIR analysis (Figure S1). And we also found that the photoluminecsence (PL) intensity of CMCDs. is strongly dependent on the reaction time (Figure S2).

5.

Figure S3. The low rate TEM image (a) and the particle size distribution (b) of the CMCD.

6.

Figure S4. The high-resolution C1s spectrum analysis of the CMCD.

Data notes:

The C1s spectrum (Figure S4) shows four peaks at 284.6, 285.7, 286.1, and 278.8 eV, which are attributed to C-C, C-N, C-O, and C=N/C=O, respectively. [S1, S3]

7.

8.

Figure S5. The UV/Vis absorption of CMCD in aqueous solution.

8.

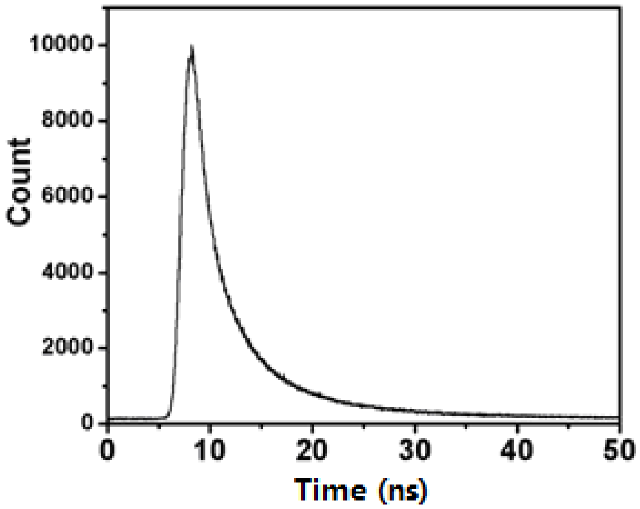

Figure S6. Luminescence decay curve of CMCD recorded at room temperature in aqueous solution.

Data notes:

The emission decay curve was monitored under the excitation wavelength at 360 nm, and the curve can be fitted by triexponential functions: τ_1 = 0.97 ns (20.47%); τ_2 = 3.70 ns (50.69%); τ_3 = 12.14 ns (28.84%). The average lifetime <τ> is estimated to be 8.90 nm by the following equation:

where A_i is the preexponential factor related to the statistical weights of each exponential and τ_i represent the lifetimes of each exponential decay.[S4]

9.

11.

Figure S7. The time-dependence with a Xe lamp of photoluminescence intensity on CMCD. PL wavelength at 450 nm (λ_{ex} = 365 nm).

10.

Figure S8. Effects of pH on the photoluminescence (PL) intensities of the raw CMCD (λ_{ex} = 365 nm).

11.

13.

Figure S9. The normalized effect of pH on the PL intensities at the emission of 450 nm of the raw CMCD.

12.

Figure S10. Plot of the relationship between pH and zeta potential.

13.

14.

Figure S11. The particle size distributions of the four E-CMCD fractions.

14.

15.

Figure S12. The analysis of the high-resolution C1s spectrum of the four E-CMCD fractions.

Data notes:

The C1s spectrum (Figure S10) shows four peaks at 284.6, 285.7, 286.1, and 278.8 eV, which are attributed to C-C, C-N, C-O, and C=N/C=O, respectively. [S1, S3]

15.

Figure S13. The possible mechanism of separating CMCD using "gradient extraction" process.

16.

Figure S14. The UV/Vis spectra of the four E-CMCD fractions in aqueous solution.

17.

Table S2 Summary of luminescence properties of the four E-CMCD fractions in aqueous solution.

	$\lambda_{em,365}$	$\lambda_{ex,450}$	$\lambda_{ex,max}$	$\lambda_{em,max}$	QY
E-CMCD$_a$	438 nm	361 nm	358 nm	438 nm	9.70 %
E-CMCD$_b$	445 nm	369 nm	363 nm	445 nm	8.64 %
E-CMCD$_c$	452 nm	380 nm	370 nm	451 nm	7.73 %
E-CMCD$_d$	456 nm	385 nm	375 nm	460 nm	8.37 %

Notes: $\lambda_{em,365}$, the emission peak at the excited wavelength of 365 nm. $\lambda_{ex,450}$, the excitation peak at the emission wavelength of 450 nm. $\lambda_{ex,max}$, the maximum excitation wavelength. $\lambda_{em,max}$ the maximum emission wavelength. QY, the quantum yield.

18.

Figure S15. The cyclic voltammogram of the E-CMCD and 0.1 mol/L KCl aqueous solution.

Data notes:

To estimate their HOMO and LUMO energy levels, cyclic voltammetry (CV) was carried out by using a standard three-electrode system, which consisted of glassy carbon electrode as the working electrode, a platinum wire as the counter electrode, and calomel electrode as the reference electrode. CV was recorded in DI-water containing CMCD and 0.1 M KCl as the supporting electrolyte. The HOMO and LUMO energy levels in eV of CMCD were calculated according to the following equations:

$$E(\mathrm{HOMO}) = -\mathrm{e}(E_{\mathrm{ox}}+4.4)\ (\mathrm{eV}) \tag{1}$$

$$E(\mathrm{LUMO}) = -\mathrm{e}(E_{\mathrm{red}}+4.4)(\mathrm{eV}) \tag{2}$$

$$E_{\mathrm{g}}=-\mathrm{e}\Delta E \tag{3}$$

$$\Delta E = E_{\mathrm{ox}}-E_{\mathrm{red}} \tag{4}$$

Where E_{ox} and E_{red} are the onset of oxidation and reduction potential, E_{g} is the energy gap, respectively.[S5]

Finally, we could calculate the energy gaps listed as below:

$E_{g,a} = 3.32$ eV, $E_{g,b} = 3.28$ eV, $E_{g,c} = 3.23$ eV, $E_{g,d} = 3.18$ eV

Where $E_{g,a}$, $E_{g,b}$, $E_{g,c}$ and $E_{g,d}$ are the energy gaps of E-CMCD$_a$, E-CMCD$_b$, E-CMCD$_c$, and E-CMCD$_d$, respectively.

19.

20.

Figure S16. Excitation-dependent PL intensities of the four E-CMCD fractions.

20.

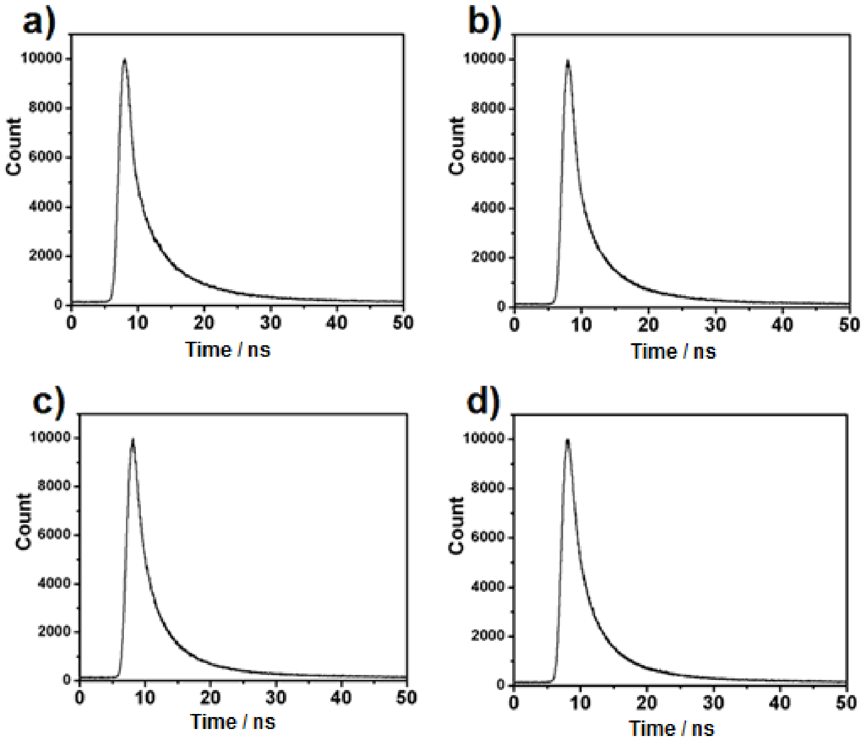

Figure S17. Fluorescence decay curve of the four E-CMCD fractions recorded at room temperature in aqueous solution. **Note:** The emission decay curve was monitored under the excitation wavelength at 360 nm, and the curves all can be fitted by triexponential functions.

21.

Figure S18. The PL behavior of the four CMCD fractions in different pH conditions.

References

[S1] J. Wang, C. F. Wang, S. Chen, *Angew. Chem. Int. Ed.* **2012**, *51*, 9297-9301.

[S2] S. Sahu, B. Behera, T. K. Maiti, S. Mohapatra, *Chem. Commun.* **2012**, *48*, 8835-8837.

[S3] Y. Deng, D. Zhao, X. Chen, F. Wang, H. Song, D. Shen, *Chem. Commun.* **2013**, *49*, 5751-5753.

[S4] Y. F. Ma, H. P. Wang, W. S. Liu, Q. Wang, J. Xu, Y. Tang, *J. Phys. Chem. B* **2009**, *113*, 14139-14145.

[S5] S. Zhu, Q. Meng, L. Wang, J. Zhang, Y. Song, H. Jin, K. Zhang, H. Sun, H. Wang, B. Yang, *Angew.Chem. Int. Ed.* **2013**, 52, 3953-3957.